©2014

Zhong Chen

ALL RIGHTS RESERVED

A NUMERICAL STUDY OF HEAT REMOVAL FROM DATA CENTER

by

ZHONG CHEN

A thesis submitted to the

Graduate School-New Brunswick

Rutgers, The State University of New Jersey

In partial fulfillment of the requirements

For the degree of

Master of Science

Graduate Program in Mechanical and Aerospace Engineering

Written under the direction of

Yogesh Jaluria

And approved by

_____

_____

_____

New Brunswick, New Jersey

October, 2014

ABSTRACT OF THE THESIS

A Numerical Study on Heat Removal from Data Centers

By ZHONG CHEN

Thesis Director:

Yogesh Jaluria

In this work, the physical problem associated with heat removal from data centers is studied. The governing equations and boundary conditions are written and solved numerically using the commercial code Fluent. The model is validated via a classic benchmark problem: natural convection in a square cavity. The problem of cooling the different servers in a data center is discussed in detail. Three configurations of a typical data center are considered. In these configurations, the data center has different locations of the outlet, and all other dimensions are kept the same. Two conditions of constant temperature and constant heat input are considered. The inlet flow velocity, the strength of server volume heat source and the temperature of server are chosen as the main variables during the simulations. By comparing the Nusselt Numbers and the dimensionless temperatures at the surfaces of the servers, the configuration with the best cooling characteristics is determined. The temperature and velocity fields in the data center are given to explain the native of the basic principle and the theory behind the differences among the three configurations.

1 Motivation

Data centers are extensively used by information technology (IT) companies, from the giant search engine Google to the digital games store Steam. It stores, manages and sends back data, which ensures that these companies function properly. As the scale of data center keeps increasing, the energy it consumes can no more be ignored. A rack of servers may take only a few KW. But if we consider the whole facility, it could take several tens of MW [1]. Some facilities have power requirements more than 100 times that of a typical office building [2]. According to the US Environmental Protection Agency, the electricity consumed by servers and data centers has grown significantly since 2000 [3]. Patterson [4] mentioned that the fast increasing power density in data centers poses a challenge to HVAC system. Tschudi [5] reported that, in a traditional distributed air-cooled computer room, the energy consumed by the HVAC system could be as high as 54% of the total energy consumed by the data center, while in a carefully designed data center, that ratio could be reduced to 22.4%. Thus, it is necessary to explore how to model and design an efficient data center cooling system.

Just like the increase in the scale of data centers, the ability of computers has also improved significantly since the day they were invented. Based on computer advances, Computational Fluid Dynamic (CFD) is widely applied in today's data center design. Patel [6] explored how CFD techniques can be applied to the high heat loads in data centers. Karki [7] applied CFD modeling to simulate raised-floor data centers with perforated tiles. Choi [8, 9] studied how different load conditions could affect the thermal profile with a CFD based tool, called ThermoStat. Chen [10] points out the effects of high power consumption manifest not only in the cost spent in designing effective cooling systems, but also in the cost of electricity consumption itself. Schmidt [11, 12] mentioned numerical analysis will exaggerate the hot and cold points in a real data center. To solve

that problem, Abdelmaksoud [13, 14] further improved CFD model, including modeling of the perforated tile flow and rack exhaust flow to conserve both mass and momentum, which reduced the difference between numerical simulation and experiments. Zhang [15] studied the energy consumption of the cooling system under different loads and the thermal response of data center cooling system.

In this thesis, the problem of improving the cooling performance of the various servers is considered. As we know, during the process of cooling, the cold flow coming from inlet absorbs heat energy from servers, resulting in its temperature increases. For that reason, the cooling effect on the server that is farthest away from the inlet is expected to be worse than that of server close to inlet. Greenberg [16] mentioned one of the best practices for data center cooling is improved air management. Enhancing data center efficiency in this way is attractive because improving air management involves less cost compared to other methods, for example, decreasing temperature of cooling flow, increasing velocity of cooling flow and so on. In this thesis, by changing the location of the outlet, the air flow velocity field is changed accordingly. Comparing the temperatures and Nusselt numbers at the surfaces of the servers, the best location of outlet is found and the theory behind that is discussed. During simulation, the inlet flow velocity, temperature of the servers and the heat load of the servers are chosen as variables. The inlet flow velocities are taken as 0.4m/s, 0.6m/s, 0.8m/s, 1m/s and 1.2m/s, the corresponding Reynolds Numbers (Re) being 5000, 7500, 10000, 12500 and 15000, respectively. The temperatures of the servers have the following values: 350K, 360K and 370K. The heat loads of the servers are reflected by the strengths of volume heat source. In this thesis, the strengths of volume heat source have the following values: 1500w/m^3, 2000w/m^3 and 2500w/m^3. All these values represent typical operating condition in relatively small data centers.

2 Governing Equations

Boussinesq approximations are used in this simulation. The governing equations are the RANS equations for incompressible flow. The detailed explanations are given in [17]. The equations are:

$$\frac{\partial \bar{u}_j}{\partial x_j} = 0, \tag{2.1}$$

$$\frac{\partial \bar{u}_i}{\partial t} + \frac{\partial}{\partial x_j}\left(\bar{u}_j \bar{u}_i\right) - \frac{\partial}{\partial x_j}\left\{\upsilon_{eff}\left[\left(\frac{\partial \bar{u}_i}{\partial x_j} + \frac{\partial \bar{u}_j}{\partial x_i}\right) - \frac{2}{3}\left(\frac{\partial \bar{u}_k}{\partial x_k}\right)\delta_{ij}\right]\right\} = -\frac{\partial \bar{p}}{\partial x_i} + g_i[1 - \beta(\bar{T} - T_0)], \tag{2.2}$$

$$\frac{\partial \bar{T}}{\partial t} + \frac{\partial}{\partial x_j}\left(\bar{T}\bar{u}_j\right) - \frac{\partial}{\partial x_k}\left(\kappa_{eff}\frac{\partial \bar{T}}{\partial x_k}\right) = 0, \tag{2.3}$$

where the bar denotes the mean quantity and $\nu_{eff} = \nu_0 + \nu_t$ is the effective kinematic viscosity, where ν_0 is the kinematic viscosity and ν_t is the turbulent kinematic viscosity, β is the coefficient of thermal expansion of the fluid, g is the gravitational body force.

$$\kappa_{eff} = \frac{\nu_t}{Pr_t} + \frac{\nu_0}{Pr}, \tag{2.4}$$

where $Pr = c_p\mu_0 / k$ and $Pr_t = c_p\mu_t / k_t$, where μ_0 is dynamic viscosity, k is thermal conductivity, μ_t is turbulent dynamic viscosity and k_t is turbulent thermal conductivity.

The Standard κ-ε turbulence model is chosen to close the RANS equations [18]. 'κ' is turbulent kinetic energy, and 'ε' stands for turbulent dissipation rate.

κ and ε can be calculate via the following two equations [19]:

$$\frac{\partial}{\partial t}(\rho\kappa) + \frac{\partial}{\partial x_i}(\rho\kappa u_i) = \frac{\partial}{\partial x_j}\left[\left(\mu + \frac{\mu_t}{\sigma_k}\right)\frac{\partial \kappa}{\partial x_j}\right] + P_\kappa + P_b - \rho\varepsilon - Y_M, \tag{2.5}$$

$$\frac{\partial}{\partial t}(\rho\varepsilon) + \frac{\partial}{\partial x_i}(\rho\varepsilon u_i) = \frac{\partial}{\partial x_j}\left[\left(\mu + \frac{\mu_t}{\sigma_\varepsilon}\right)\frac{\partial \varepsilon}{\partial x_j}\right] + C_{1\varepsilon}\frac{\varepsilon}{\kappa}(P_\kappa + C_{3\varepsilon}P_b) - C_{2\varepsilon}\rho\frac{\varepsilon^2}{\kappa}, \quad (2.6)$$

where P_k represents the production of κ due to the mean velocity gradient, $P_k = -\rho\overline{u_i u_j}\frac{\partial u_j}{\partial x_j}$, P_b represents the production of κ due to buoyancy, for ideal gas, $P_b = -g_i\frac{\mu}{\rho Pr_t}\frac{\partial \rho}{\partial x_i}$. Y_m is the contribution of the fluctuating dilatation in compressible turbulence to the overall dissipation rate, which is only considered in high-Mach-number flows and is neglected in incompressible flows, Y_m=0. The turbulent viscosity (μ_t) is calculated as

$$\mu_t = \rho C_\mu \frac{\kappa^2}{\varepsilon}. \quad (2.7)$$

The model constants $C_{1\varepsilon}$, $C_{2\varepsilon}$, C_μ, σ_k and σ_ε have following values respectively: 1.44, 1.92, 0.09, 1.0 and 1.3 [19].

3 Validation

In this thesis, simulations were done with Fluent, which is part of the ANSYS software. Before turning to simulating the flow, Fluent is used to solve a classic benchmark problem, which is natural convection in a square cavity, to validate the code [20].

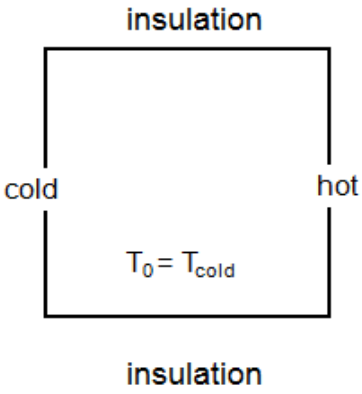

Figure 3.1. The configuration for the problem of natural convection in a square cavity.

The problem is defined as the following. Fluid fills a closed square cavity in the figure above. Side Walls are heated or cooled surfaces, while the top and bottom surfaces are insulated. Buoyancy effects are taken into account, and it drives the fluid flow in the enclosure. The Rayleigh number (Ra) is employed to indicate the strength of buoyancy, and, specifically, in this case to indicate the temperature difference between the cold and hot walls. For free convection near a vertical wall, the definition of Ra is

$$Ra_x = \frac{g\beta}{\nu\alpha}(T_s - T_\infty)x^3 \qquad (3.1)$$

where x is characteristic height, g is magnitude of acceleration due to gravity, ν is kinematic viscosity, α is thermal diffusivity, T_s is surface temperature and T_∞ is ambient temperature.

Here, typical values are chosen as g = 9.8 m/s^2, β = 0.003315 (1/K), x = 0.1m, ν = 1.6×10^5 m^2/s, α = 2.253 m^2/s. As given by de Vahl Davis [20], four cases of Ra = 10^3, 10^4, 10^5 and 10^6 were chosen. The temperature fields and contours of velocity in horizontal direction are given in Figure 3.3 to Figure 3.9.

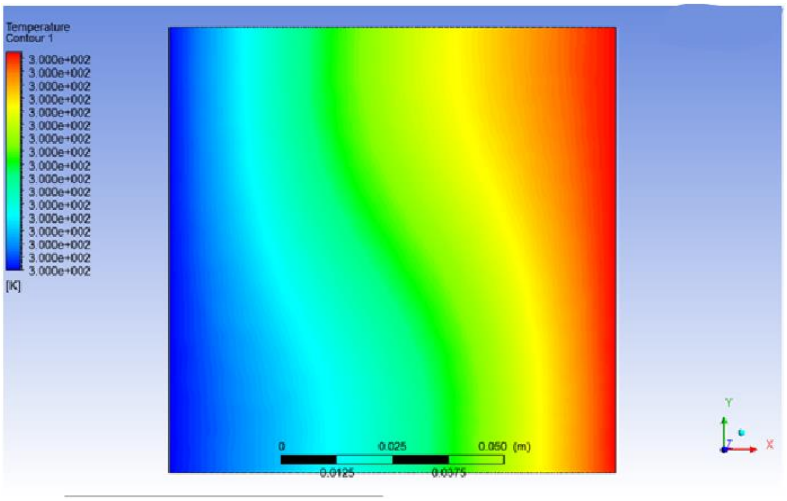

Figure 3.2. Temperature field at Ra = 10^3.

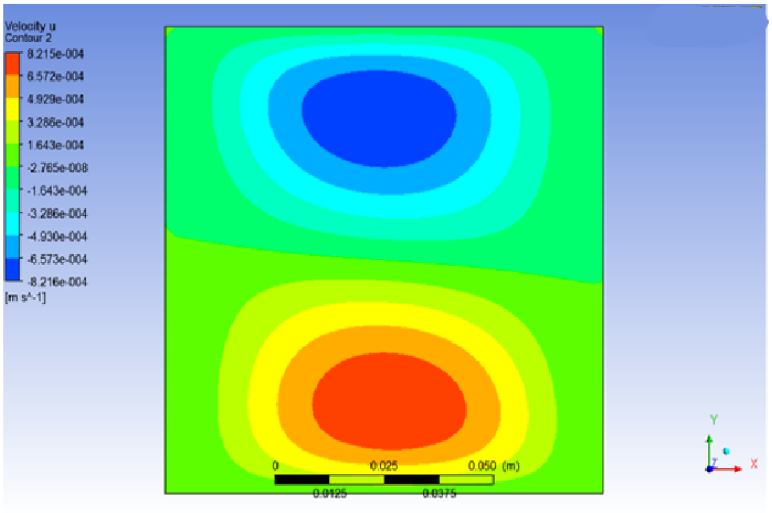

Figure 3.3. Contour of velocity in horizontal direction at Ra = 10^3.

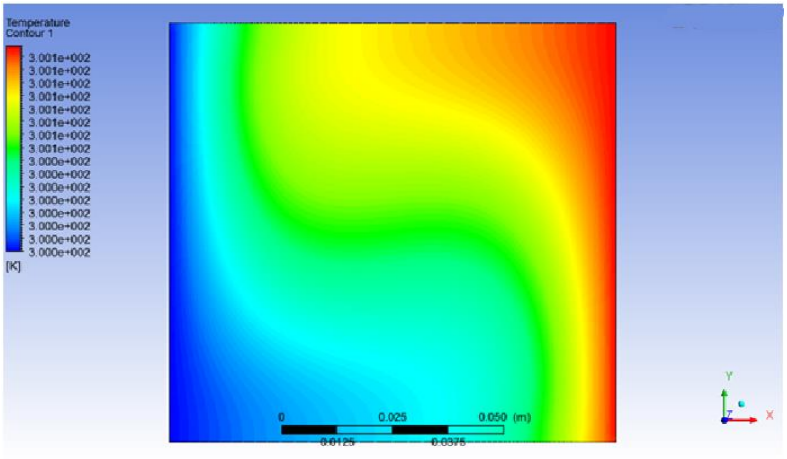

Figure 3.4. Temperature field at Ra = 10^4.

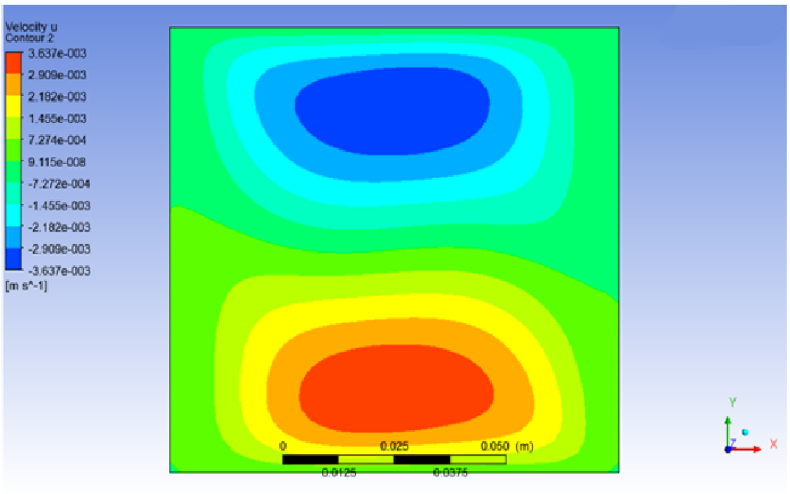

Figure 3.5. Contour of velocity in horizontal direction at Ra = 10^4.

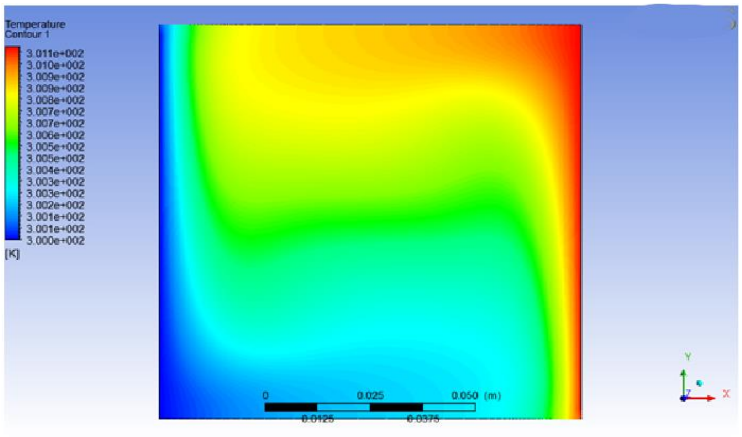

Figure 3.6. Temperature field at Ra = 10^5.

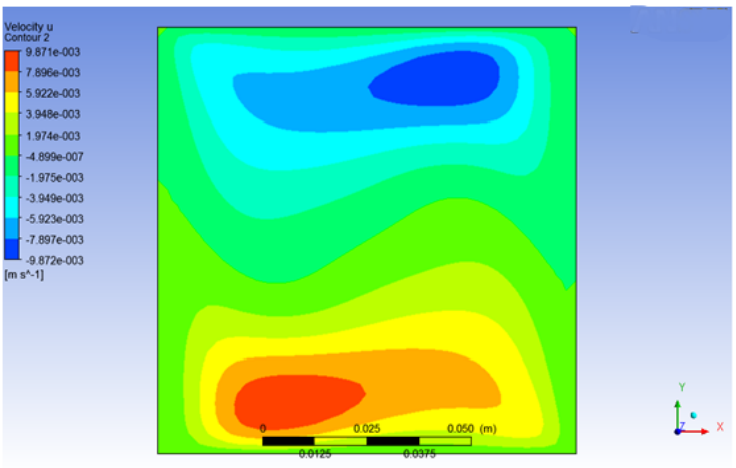

Figure 3.7. Contour of velocity in horizontal direction at Ra = 10^5.

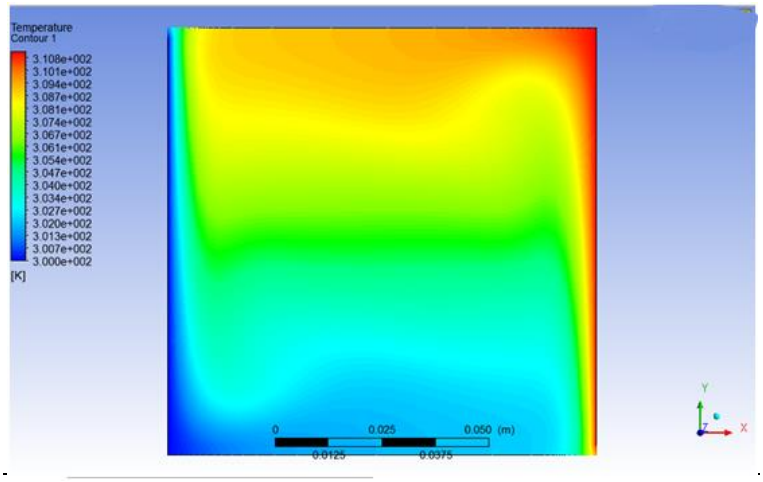

Figure 3.8. Temperature field at Ra = 10^6.

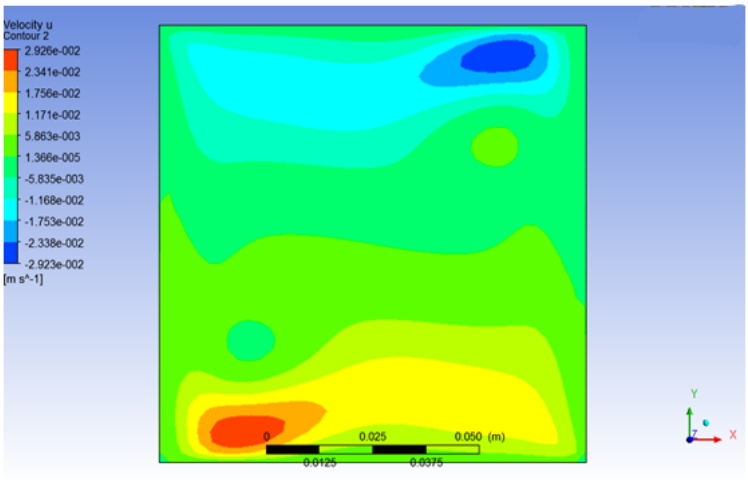

Figure 3.9. Contour of velocity in horizontal direction at Ra = 10^6.

The benchmark solutions from [20] are given in Figure 3.10 to Figure 3.13, the surface plot is temperature field, the contour depicts horizontal velocity and arrows are velocity. From Figure 3.10 to Figure 3.13, we can see that, as Ra number increasing, the buoyancy effects get stronger. When the Ra number equals to 10^3, in both the benchmark results and my simulation results, watershed line between high temperature flow and low temperature flow is a vertical line across the center of the domain. And my simulation results are close to the benchmark results at large Ra number. When the Ra number equals to 10^6, the flow in the upper half domain's temperature is obviously higher than the flow in the down half domain. That is the result of the density of high temperature flow is smaller than that of low temperature flow. We can see that the current simulation results agree well with the earlier ones. So the ANSYS simulation model may be assumed to be validated. Then we may now proceed to the data center cooling analysis.

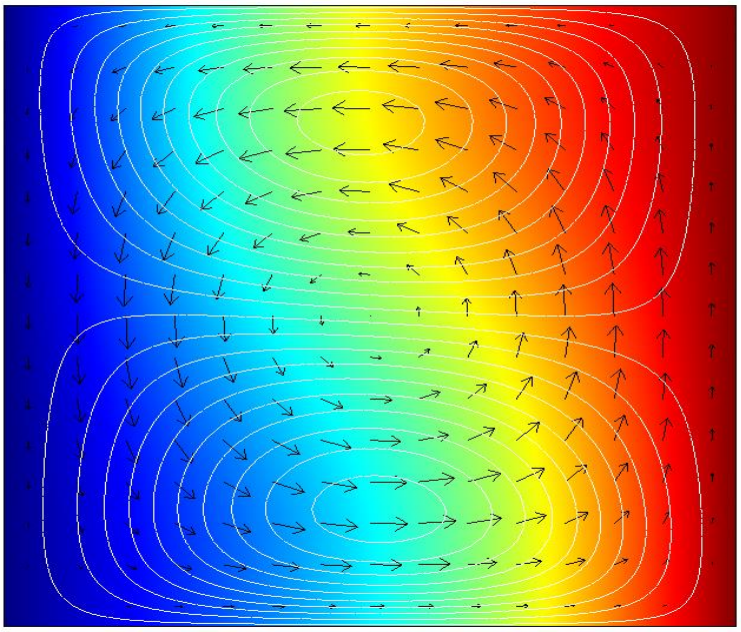

Figure 3.10. Benchmark result of temperature field, horizontal velocity and velocity at Ra = 10^3.

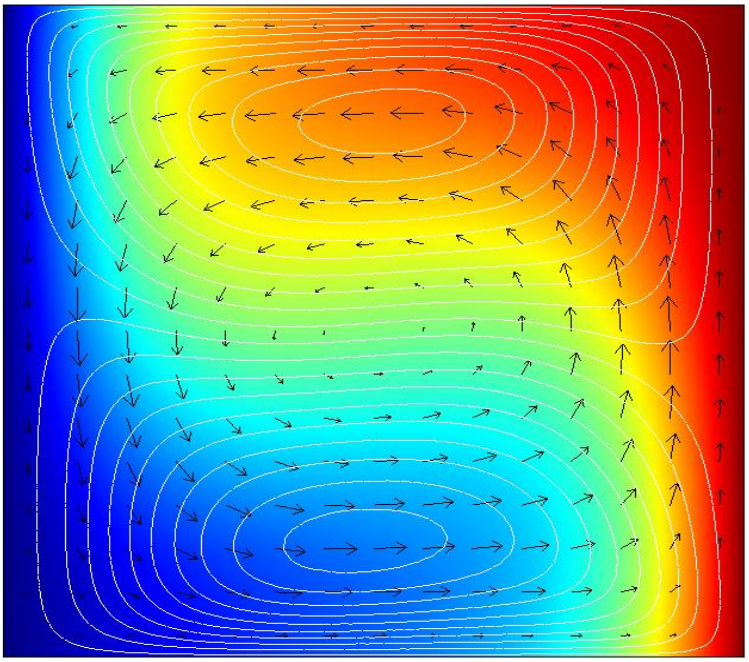

Figure 3.11. Benchmark result of temperature field, horizontal velocity and velocity at Ra = 10^4.

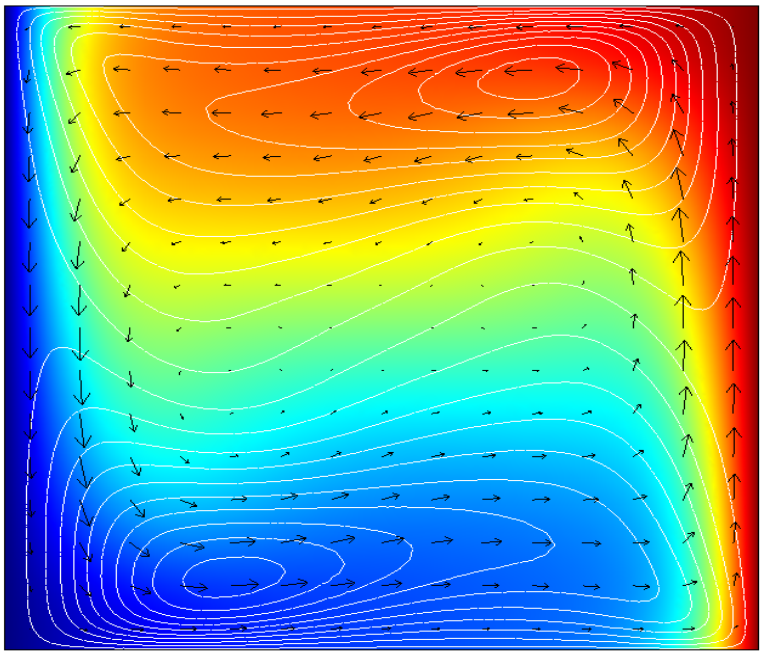

Figure 3.12. Benchmark result of temperature field, horizontal velocity and velocity at Ra = 10^5.

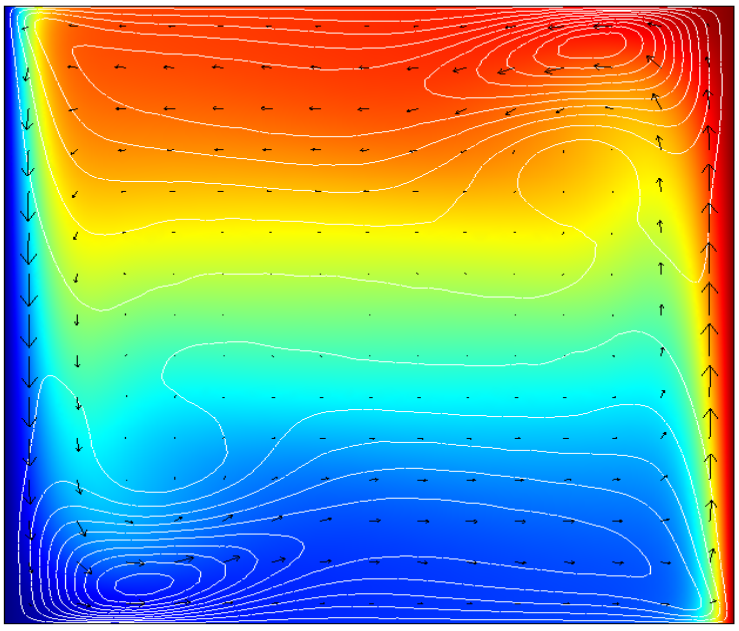

Figure 3.13. Benchmark result of temperature field, horizontal velocity and velocity at Ra = 10^6.

4 Mathematical and Numerical Model

Several configurations are considered to simulate a data center with different outlet locations.

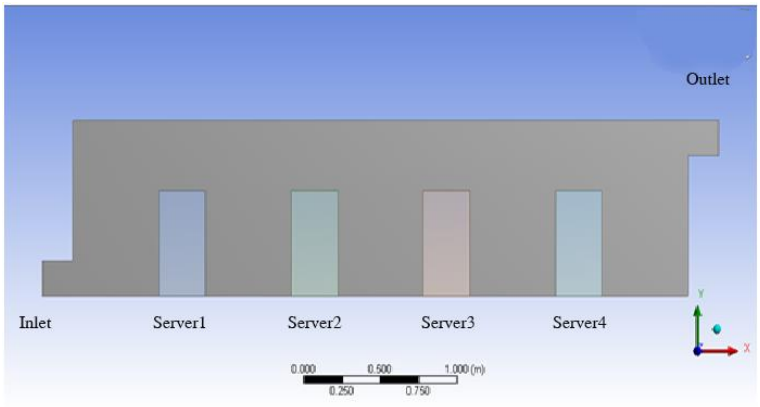

Figure 4.1. Data center of configuration 1.

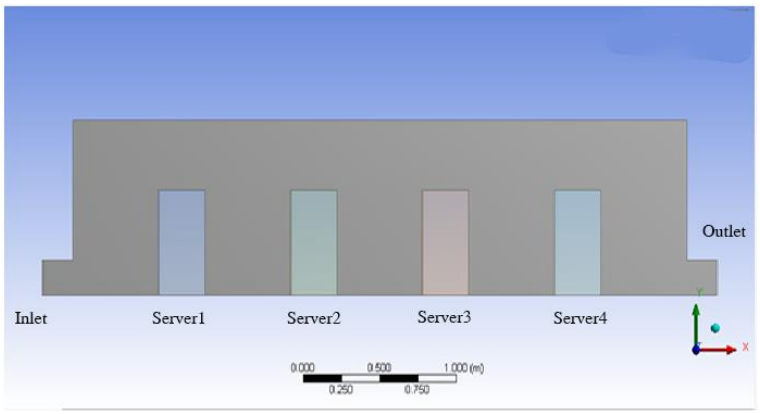

Figure 4.2. Data center of configuration 2.

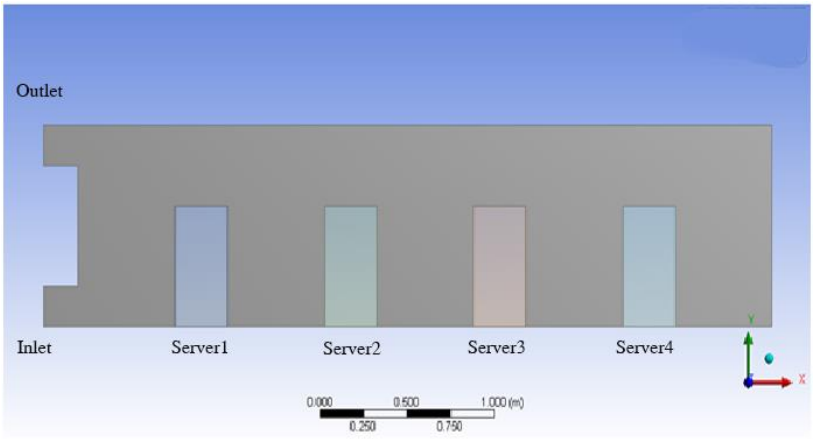

Figure 4.3. Data center of configuration 3.

As the above figures show, four servers are located on the floor of the data center. The ratio of distance between front surface of server1 and the inlet to the whole length of data center is 0.180. The corresponding ratios for server 2, server 3 and server 4 are 0.386, 0.590 and 0.800, respectively. The dimensions of the data center are taken as 4m in length and 1m in height. All the servers are of the same size, 0.6m in height and 0.3m in width. Figure 4.1 configuration 1 denotes the outlet located in upper right hand corner case, and in Figure 4.2 configuration 2 the outlet is located at the down right hand corner. Figure 4.3 configuration 3 shows the inlet and outlet are on the same side case. This configuration has the lowest cost due to reduced duct length.

Silicon is chosen as the material of the servers, and the cooling fluid is air. The temperature of the ambient environment is taken as 300K, which is also the inlet temperature. Standard k-epsilon model is used. Boussinesq approximations are included to take into account buoyancy effects. The average temperature of the fluid domain in the

data center was found to be approximately 303K for the conditions studied. The inlet boundary condition is velocity inlet, and the outlet boundary condition is taken as the outflow condition, with zero gradient in the outflow direction. In all cases, the mass conservation and energy conservation were ensured through calculations. All the walls of the data center are taken as adiabatic.

Several mesh sizes have been used in order to avoid the error brought in by a sparse mesh. In the testing case, configuration1 is picked, flow velocity at the inlet is 0.6m/s, and the volume heat source strength in each server is 2000 W/m^3. The average temperature at the outlet is taken to indicate the convergence of mesh influence.

Nodes	Elements	Temperature at Outlet(K)
1074	990	310.37
9154	8904	310.33
16161	15828	310.33

Table 4.1. Temperature at outlet vs. mesh size.

From Table 4.1, we can see that the temperature at the outlet drops from 310.37K to 310.33 when the number of element increases from 990 to 8904. However, when the number of elements increases further from 8904 to 15828, the temperature at outlet is almost the same. Taking the accuracy and running time into account, 9154 nodes and 8904 elements are used in this thesis. And the specific meshes are given in Figure 4.4 to Figure 4.6.

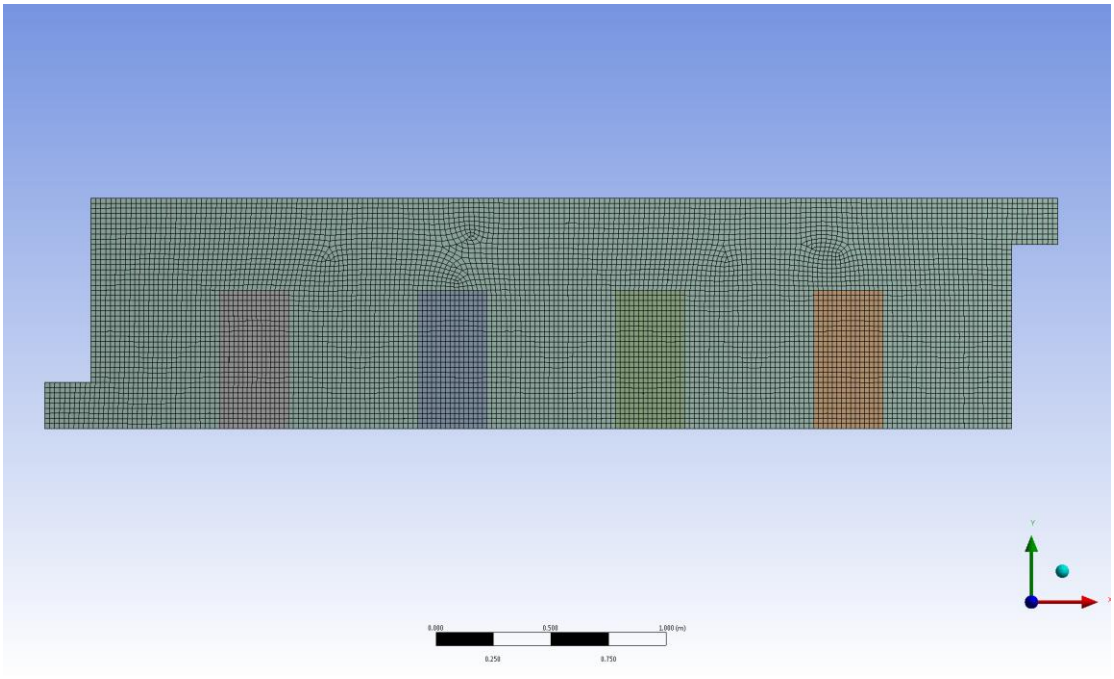

Figure 4.4 The mesh for configuration 1.

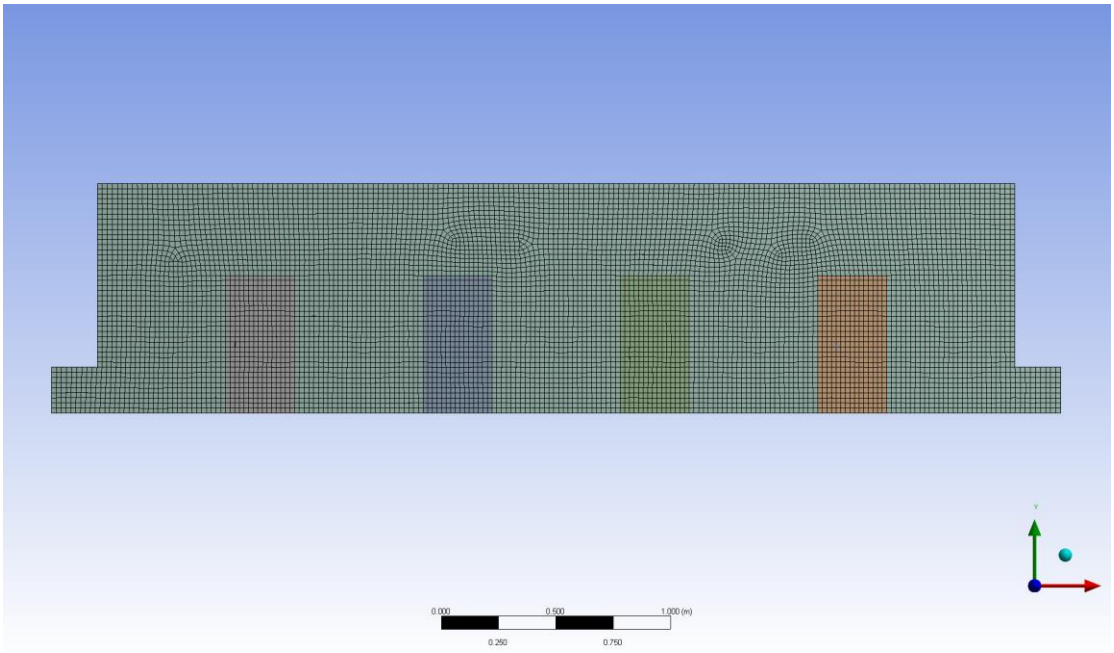

Figure 4.5. The mesh for configuration 2.

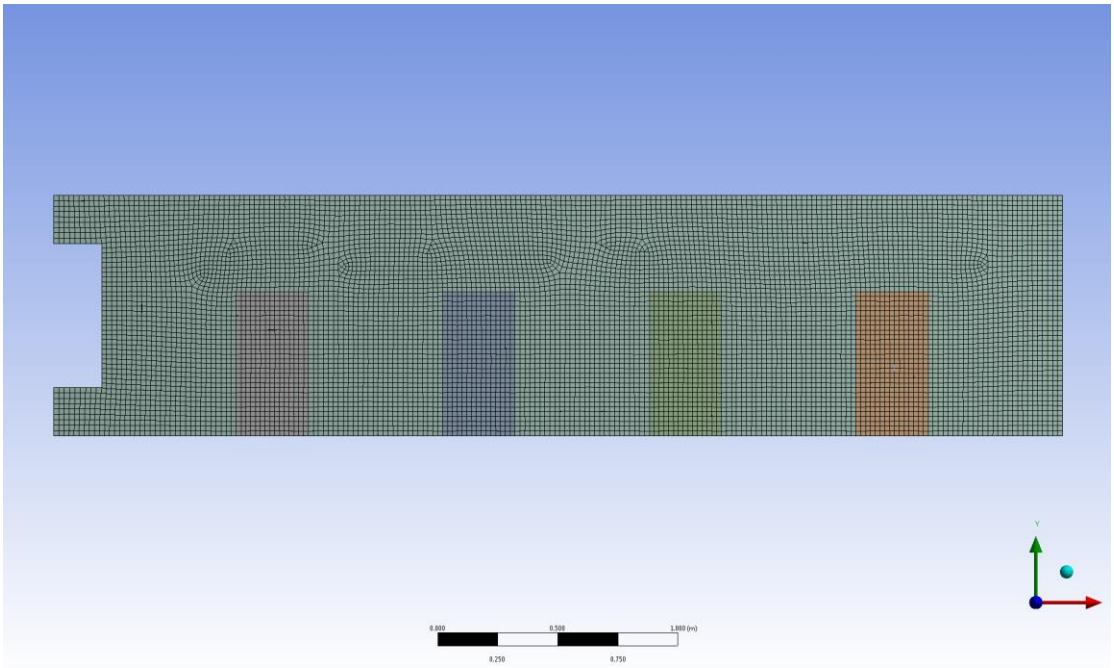

Figure 4.6 The mesh for configuration 3

5 Analysis

Before simulations are presented, some dimensionless numbers need to be introduced. First, the dimensionless temperature is defined as

$$T^* = \frac{T - T_m}{\frac{H^2 Q}{k}}, \tag{5.1}$$

where T is the physical temperature, T_m is the ambient temperature, H is the characteristic length, Q is the strength of volume heat source and k is thermal conductivity. In this thesis H is taken as the inlet length, 0.2 m.

Second, the Grashof number (Gr), which approximates the ratio of the buoyancy effects to the viscous effects, is defined as

$$\mathrm{Gr} = \frac{g\beta(T-T_m)H^3}{\upsilon^2}, \tag{5.2}$$

where g is the magnitude of acceleration due to gravity and υ is kinematic viscosity.

Last but not least, the Nusselt number (Nu), which is the ratio of convective heat transfer to conductive heat transfer, is defined as

$$\mathrm{Nu} = \frac{hH}{k}, \tag{5.3}$$

$$h = \frac{q}{T-T_m}, \tag{5.4}$$

where h is the coefficient of convective heat transfer and q is the heat flux. In this thesis, the influence of the outlet location on the cooling effect is studied by using two heat input conditions. In the first case, the strength of volume heat source is constant. In the other case, the temperature of servers is constant.

5.1 Constant volume heat source

In Figure 5.1 to Figure 5.3, the strengths of volume heat source in servers are 1500w/m^3, 2000w/m^3 and 2500w/m^3, respectively. Accordingly, the Gr for the three conditions are obtained as 1×10^{10}, 1.5×10^{10} and 2×10^{10}. During simulation, Re is chosen as 5000, 7500, 10000, 12500 and 15000. The corresponding physical velocities at the inlet are 0.4m/s, 0.6m/s, 0.8m/s, 1.0m/s and 1.2m/s. Figure 5.1 to Figure 5.3 show that, when the velocity at the inlet is increased, or in other words the Re number is increased, the servers' temperatures decrease. This result agrees with our previous understanding that a faster flow passing a surface leads to higher coefficient of convective heat transfer,

resulting in lower temperature on the surface. Besides, comparing the temperatures of different servers in the data center when under the same inlet flow velocity, we can find that the temperature of server 4 is the highest, and then are server 3, server 2 and server 1. This result is because another factor that affects the coefficient of convective heat transfer is the temperature difference. As flow successively passing server 1, server 2, server 3 and server 4, its temperature keeps climbing because absorbing heat from servers. So the cooling effect on the servers that are farther from to the inlet would be worse than that on the servers that are close to the inlet. Another observation is that, as the Re increases, the slopes of temperature of server 2 and server 3 are smaller than those of serve 1 and server 4. The reason for that is because the server 2 and 3 are located between the server 1 and server 4 in the data center. So that, even the flow rate of inlet flow increases, the local flow rates that passes server 2 and server 3 does not increase as much as that flowing server 1 and server 4.

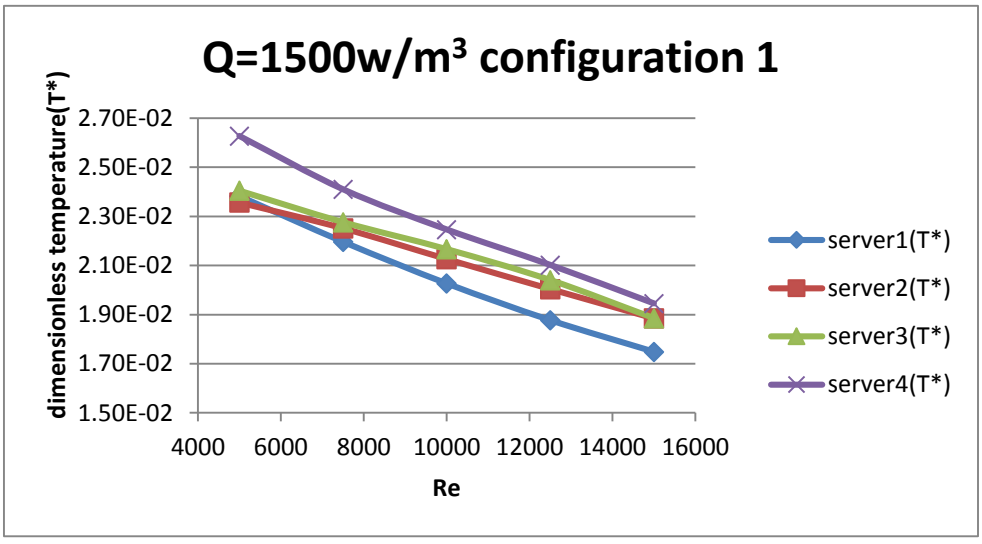

Figure 5.1. Dimensionless temperature as a function of the Re number for configuration 1 for different servers at Q=1500w/m³.

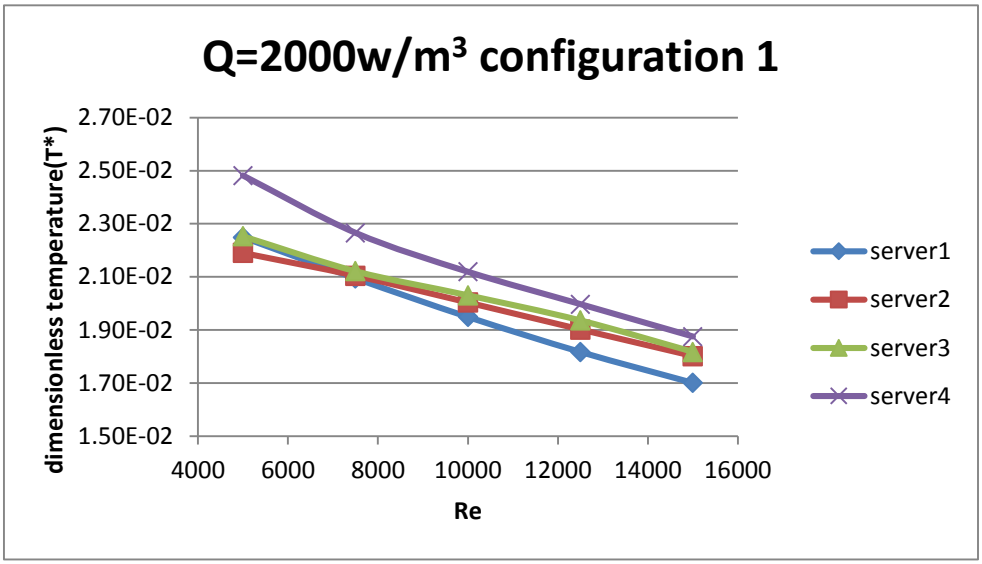

Figure 5.2. Dimensionless temperature as a function of the Re number for configuration 1 for different servers at Q=2000w/m^3.

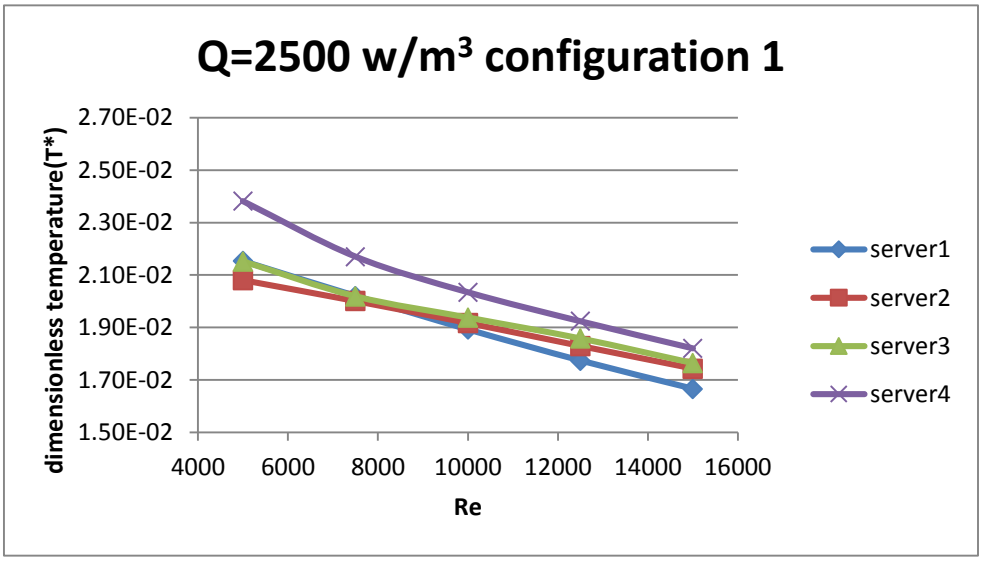

Figure 5.3. Dimensionless temperature as a function of the Re number for configuration 1 for different servers at Q=2500w/m^3.

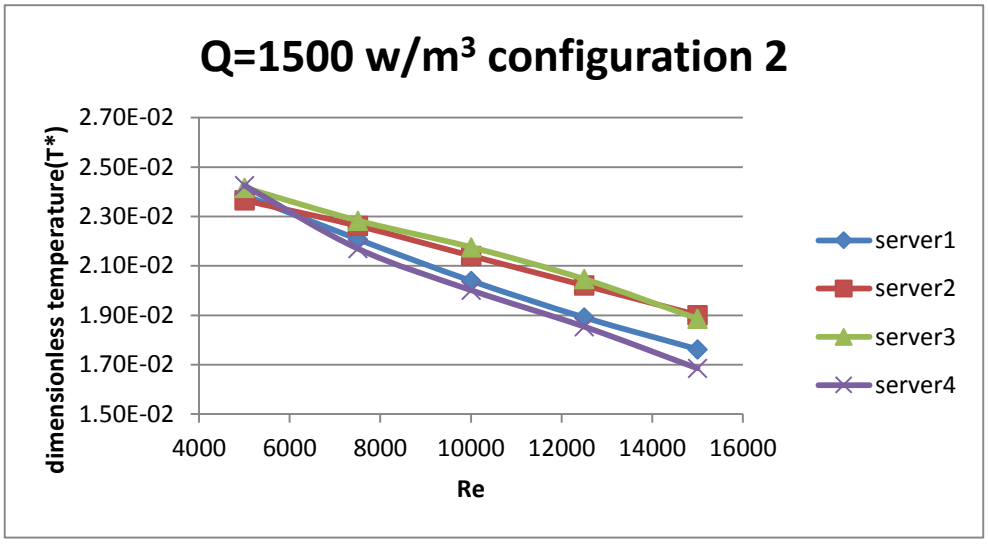

Figure 5.4. Dimensionless temperature as a function of the Re number for configuration 2 for different servers at Q=1500w/m^3.

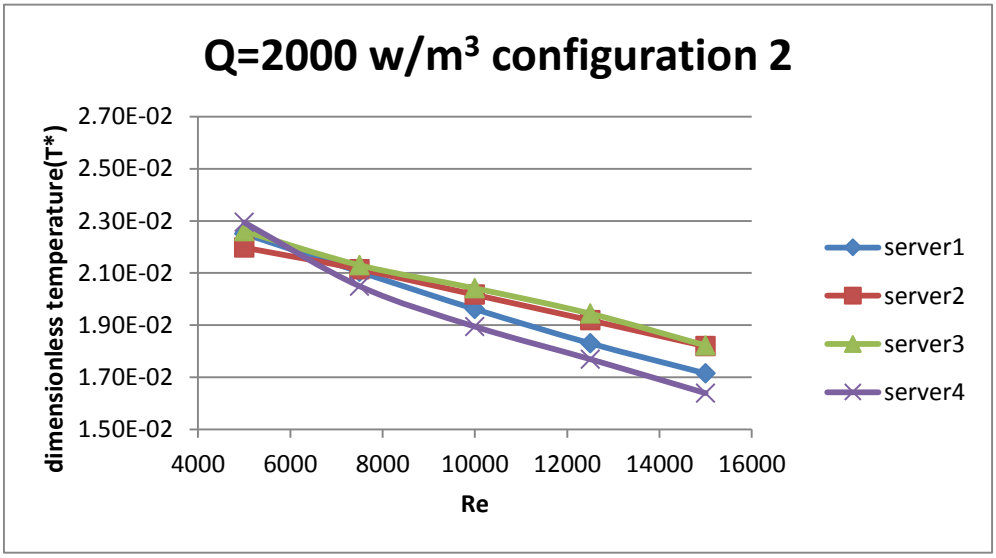

Figure 5.5. Dimensionless temperature as a function of the Re number for configuration 2 for different servers at Q=2000w/m^3.

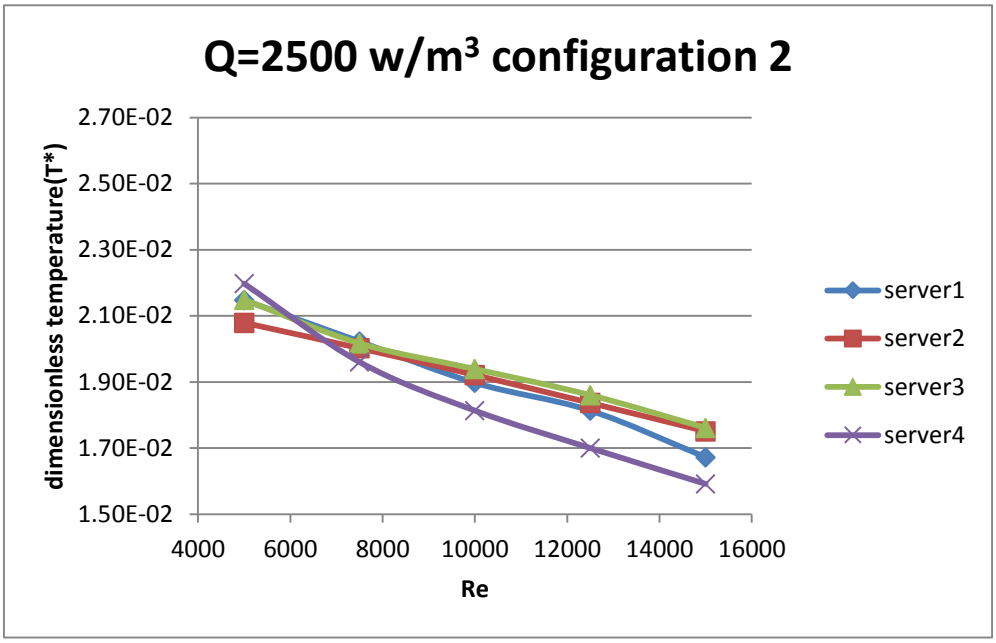

Figure 5.6. Dimensionless temperature as a function of the Re number for configuration 2 for different servers at Q=2500w/m3.

Figure 5.4 to Figure 5.6 show cases under the same simulating conditions in Figure 5.1 to Figure 5.3, but the configuration is different. The location of outlet changes from upper right hand side to down right hand side. Comparing to Figure 5.1 to Figure 5.3, we can find that the temperature of server 4 drops significantly in Figure 5.4 to Figure 5.6. In the Figure 5.1 to Figure 5.3, the server 4's temperature is highest among all servers. While in the Figure 5.4 to Figure 5.6, the cooling effect on server 4 is the best. This observation is useful in designing a data center, which significantly improves the cooling effect on the rear servers. Besides, the temperatures of other servers do not change very much. In the configuration 2, the condition of incoming flow, when passing server 1, 2 and 3, is nearly the same as in the configuration 1.

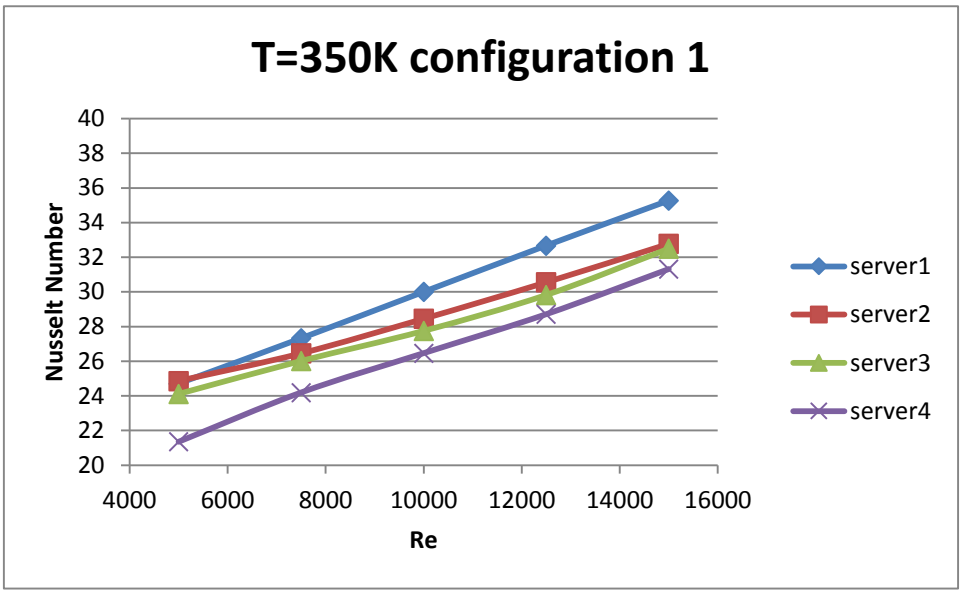

Figure 5.7. Nusselt number as a function of the Re number for configuration 1 for different servers at server temperature (T) = 350K.

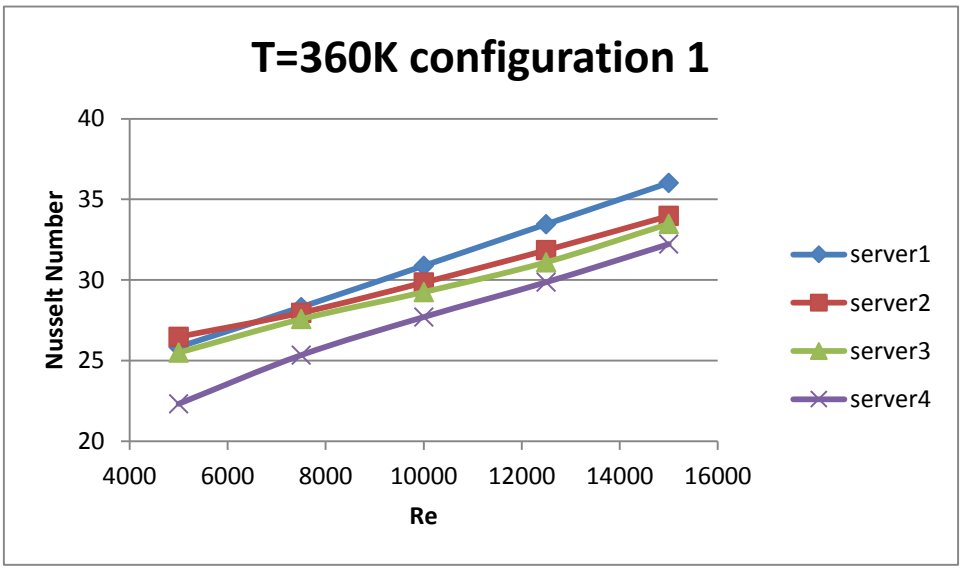

Figure 5.8. Nusselt number as a function of the Re number for configuration 1 for different servers at server temperature (T) = 360K.

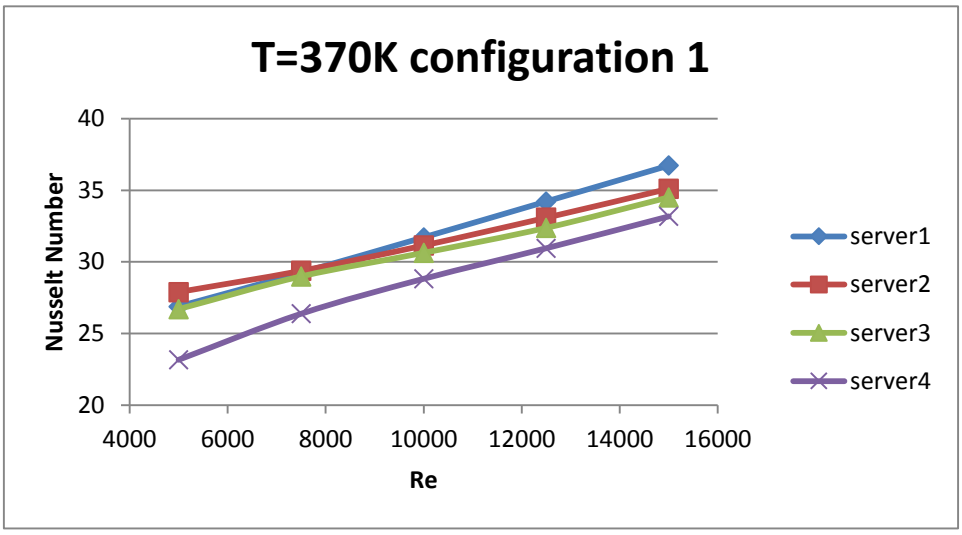

Figure 5.9. Nusselt number as a function of the Re number for configuration 1 for different servers at server temperature (T) = 370K.

5.2 Server temperature constant

In Figure 5.7 to Figure 5.9, the temperature of the servers is held constant in each figure. When the temperatures of servers are 350K, 360K and 370K, the Gr calculated as 5×10^8, 6×10^8 and 7×10^8, respectively. As the inlet flow velocity increased, the Nu increases, which indicated that the heat convection at the surface of servers gets stronger. Besides, under the same inlet flow, the server1's Nu is the highest, and then are server 2, server 3 and server 4. Similar to the constant volume heat source cases, the server 2 and server 3 are less sensitive to incoming flow velocity than server 1 and server 4. And the reason for cooling effect difference on the servers is again the different distances from inlet to each server. The closer a server is to the inlet, it is cooled by the lower temperature flow. The result of different sensitivities to incoming flow velocity is due to

the exterior servers (server 1 and server 4) being exposed to the flow more than the interior servers (server 2 and server 3).

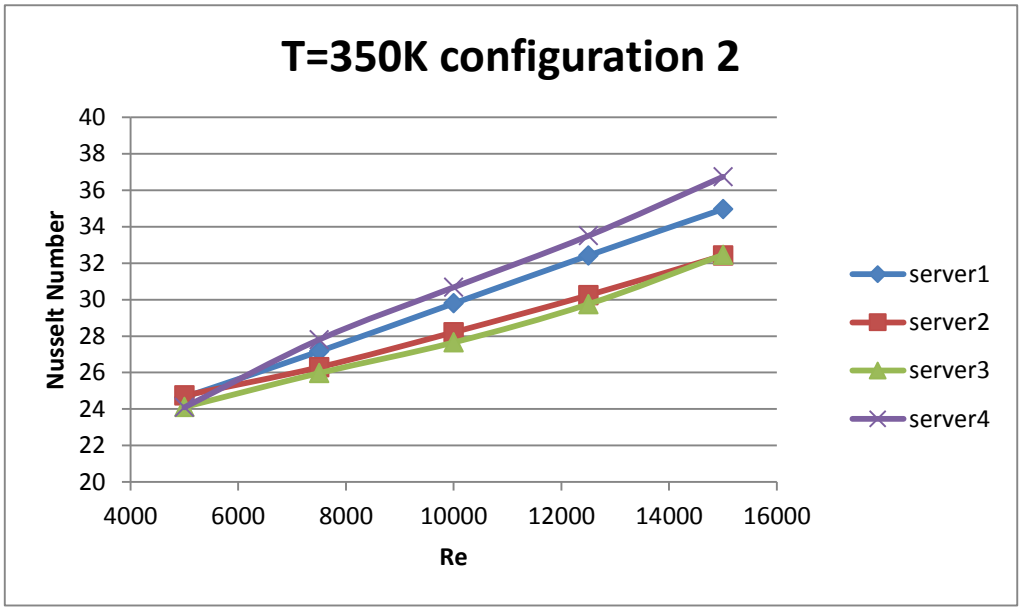

Figure 5.10. Nusselt number as a function of the Re number for configuration 2 for different servers at server temperature (T) = 350K.

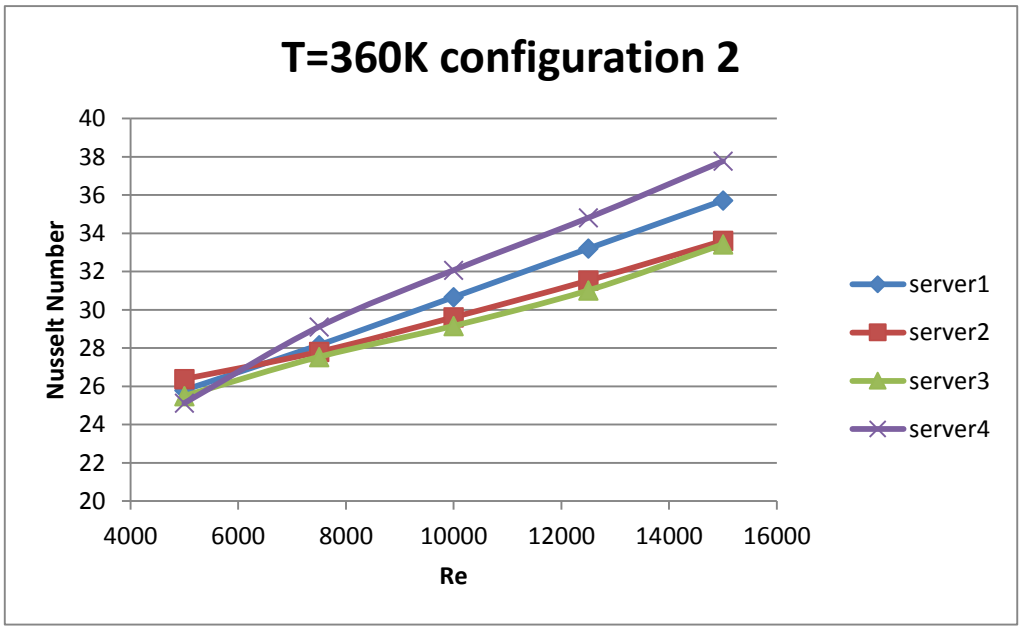

Figure 5.11. Nusselt number as a function of the Re number for configuration 2 for different servers at server temperature (T) = 360K.

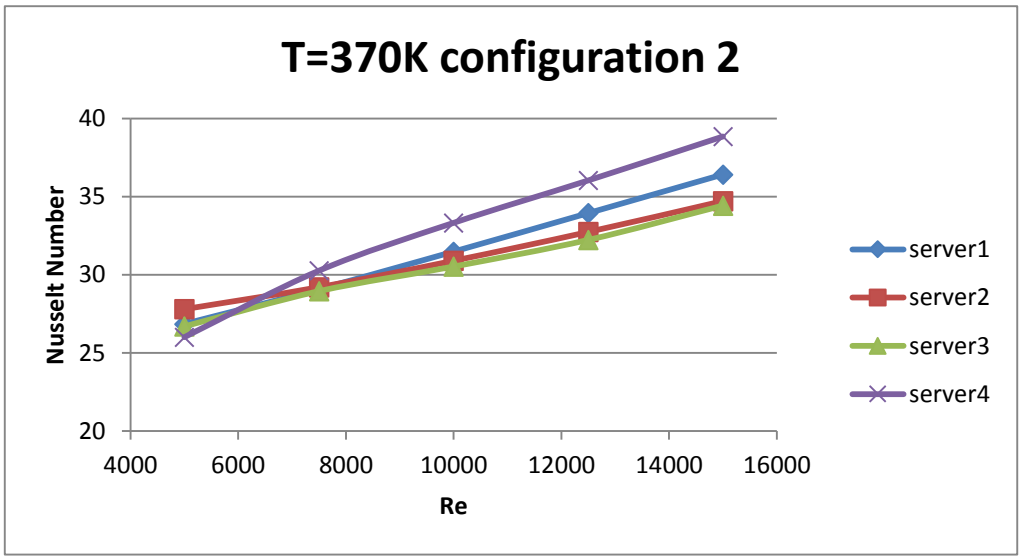

Figure 5.12. Nusselt number as a function of the Re number for configuration 2 for different servers at server temperature (T) = 370K.

In Figure 5.10 to Figure 5.12, configuration 2, in which case the outlet is located the down right hand side, is used. In these figures, one obvious difference to Figure 5.6 to Figure 5.9 is the Nu of server 4. In Figure 5.6 to Figure 5.9, the server 4's Nu is lowest, meaning the heat convection effect of server 4 is worst. While in Figure 5.10 to Figure 5.12, after changing the location of outlet, the Nu number of server 4 becomes the highest. Besides, the influences of changing the location of outlet on servers other than server 4 are small.

5.3 The temperature of servers under different heat fluxes

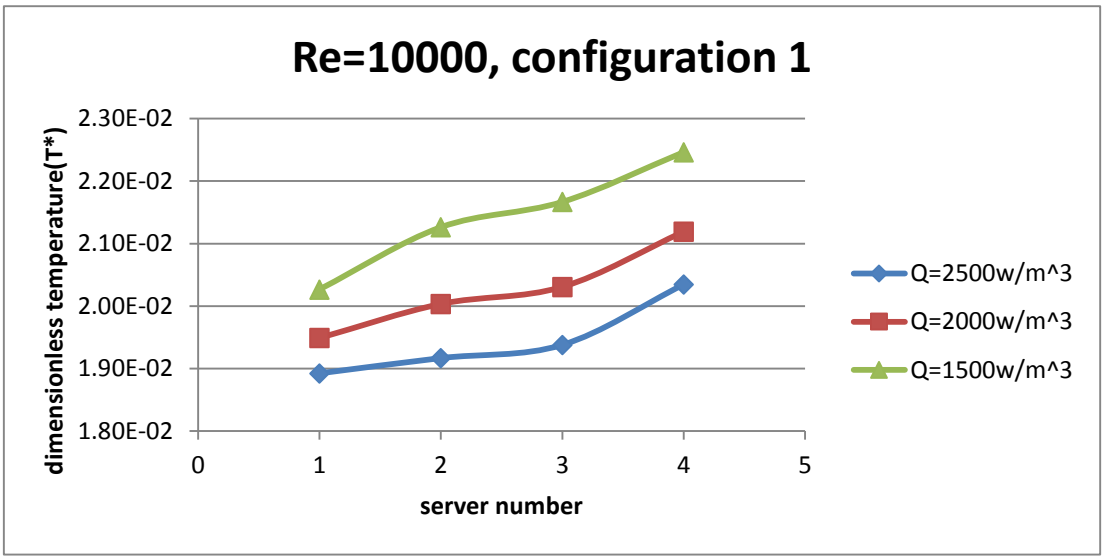

Figure 5.13. Servers dimensionless temperature under different strengths of volume heat source at Re = 10000, configuration 1.

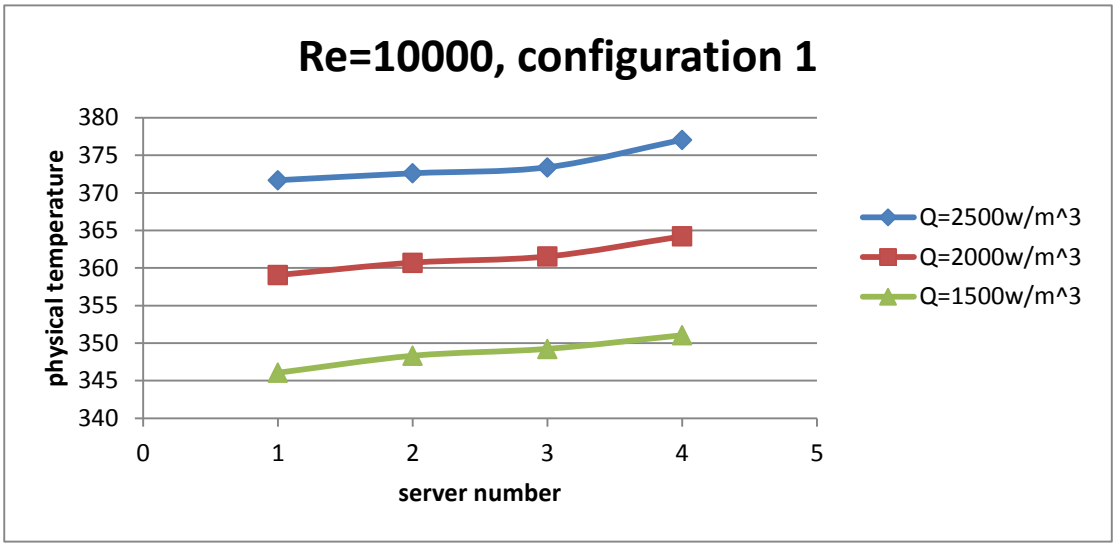

Figure 5.14. Servers physical temperature under different strengths of volume heat source at Re = 10000, configuration 1.

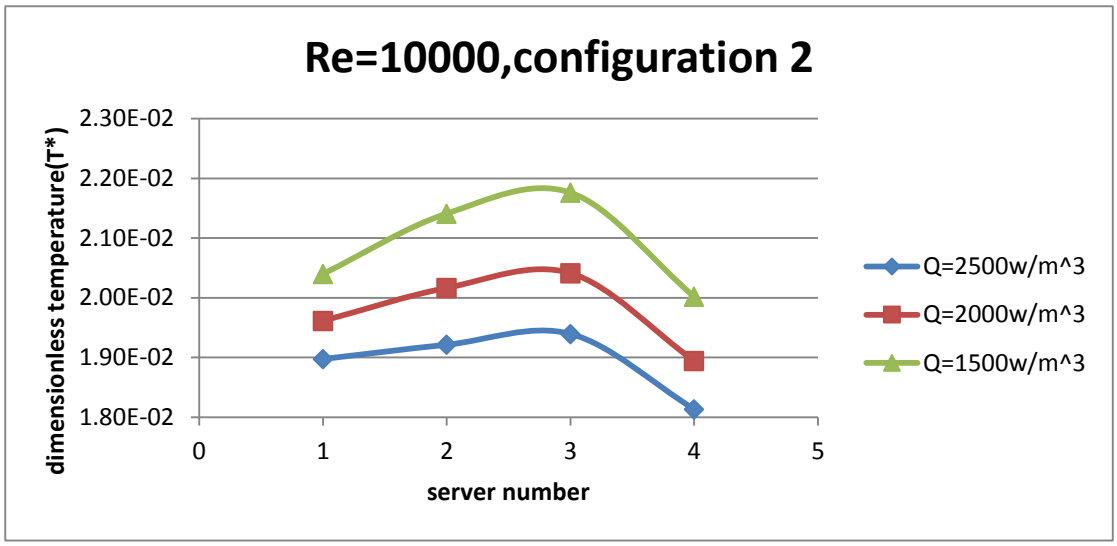

Figure 5.15. Servers dimensionless temperature under different strengths of volume heat source at Re = 10000, configuration 2.

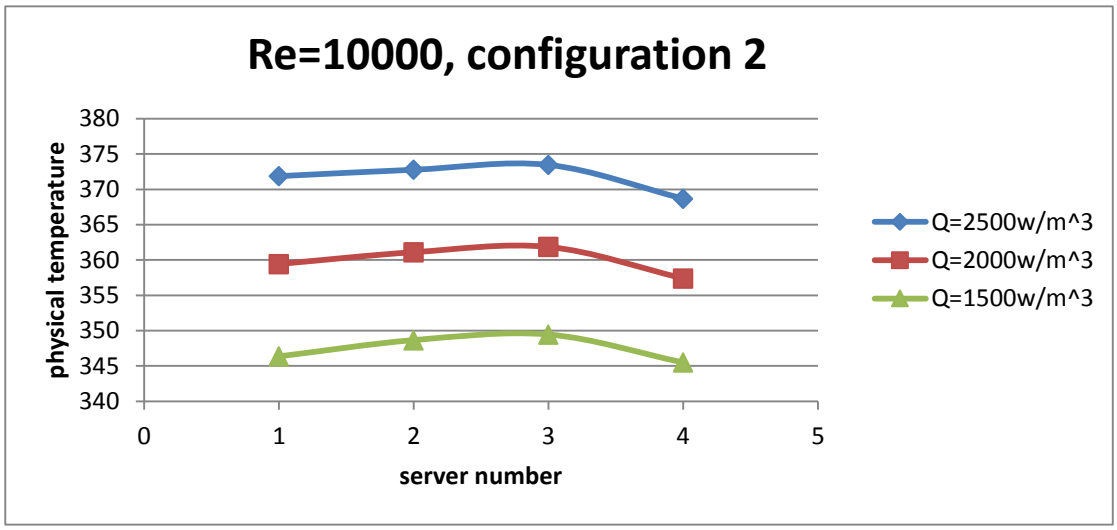

Figure 5.16. Servers physical temperature under different strengths of volume heat source at Re = 10000, configuration 2.

In this section, different strengths of volume heat source are applied to the servers, while the inlet velocity is remained the same. Figure 5.13 and Figure 5.14 are the configuration 1 cases, and Figure 5.15 and Figure 5.16 are the configuration 2 cases. Both dimensionless temperature and physical temperature are calculated. From the above figures we can see server temperatures converge to a small range when transferring from physical temperature to dimensionless one, which means by using dimensionless parameters the results could represent a series of experiment conditions.

From Figure 5.14 and Figure 5.16, we can find the physical temperature ranges in the simulation cases are from 340K to 380K, which is the practical operation temperature of servers. Besides, by comparing Figure 5.13 and Figure 5.15, the difference of the server 4 temperature dues to different configurations is obvious. In configuration 2, the server 4 even has lower temperature than server 1, while in configuration 1 the server 4 has the highest temperature among all the servers.

5.4 Temperature and velocity fields

In this section, the temperature fields of different configurations are studied. The inlet flow velocity is held Re=7500 (v = 0.6m/s). And the severs temperature is changing from 350K to 370K. From Figure 5.17 to Figure 5.18, we can see that the domain between server 3 and server 4 is the area that is most sensitive to server temperature increasing. As the server temperature keeps increasing to 370K, the domain between server 3 and server 4 remains the most dangerous area, also called hot spots. So in the process of designing a data center, a specific attention should be paid to that area.

In Figure 5.20 to Figure 5.22, configuration 2 was used. We can see a similar dangerous domain between server 3 and server 4. But there is a big difference in the domain between the server 4 and outlet. In Figure 5.19, the low temperature flow does not touch the domain behind the server 4 and goes out from the outlet directly. While in the Figure 5.22, the relatively cold flow has to go through the domain behind server 4, for the reason that the location of outlet moves from the upper right hand side to the down right

hand side. This path significantly enhances the interaction between the low temperature flow and server 4, which leads to a much better cooling effect on the server 4.

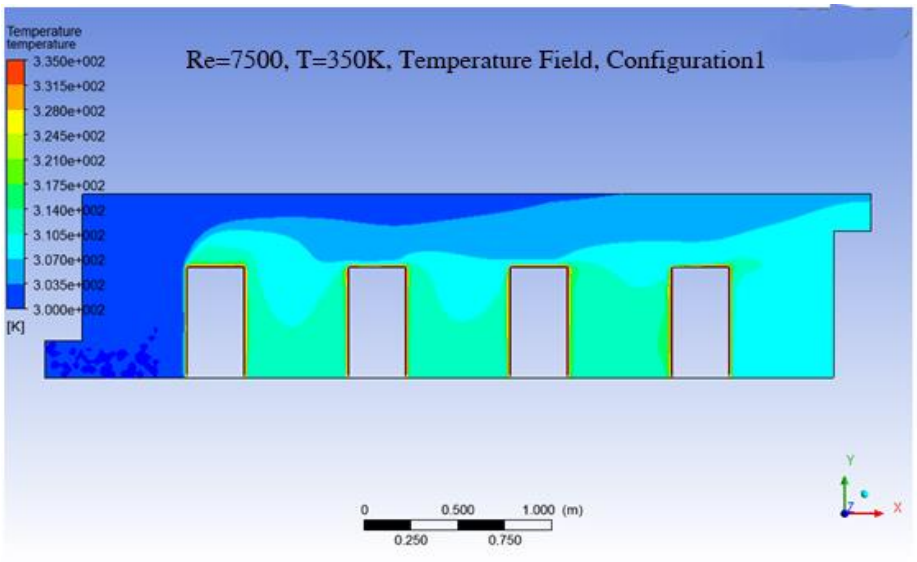

Figure 5.17. Temperature field of data center at Re = 7500 and server temperature (T) = 350K, configuration 1.

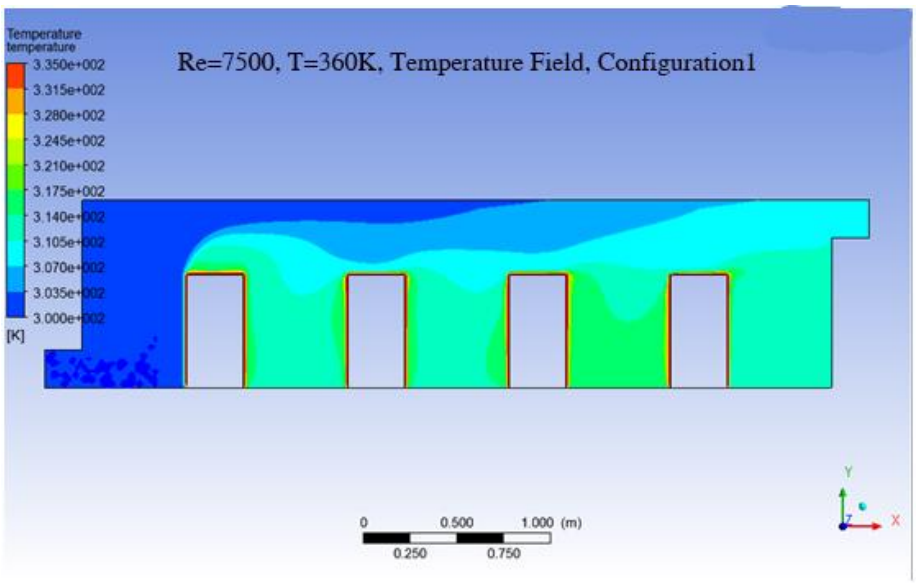

Figure 5.18. Temperature field of data center at Re = 7500 and server temperature (T) = 360K, configuration 1.

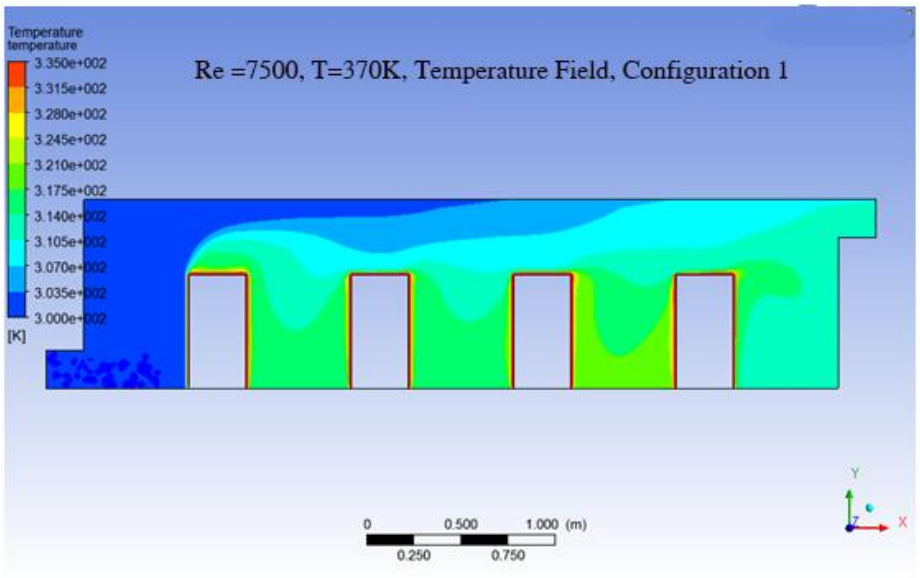

Figure 5.19. Temperature field of data center at Re = 7500 and server temperature (T) = 370K, configuration 1.

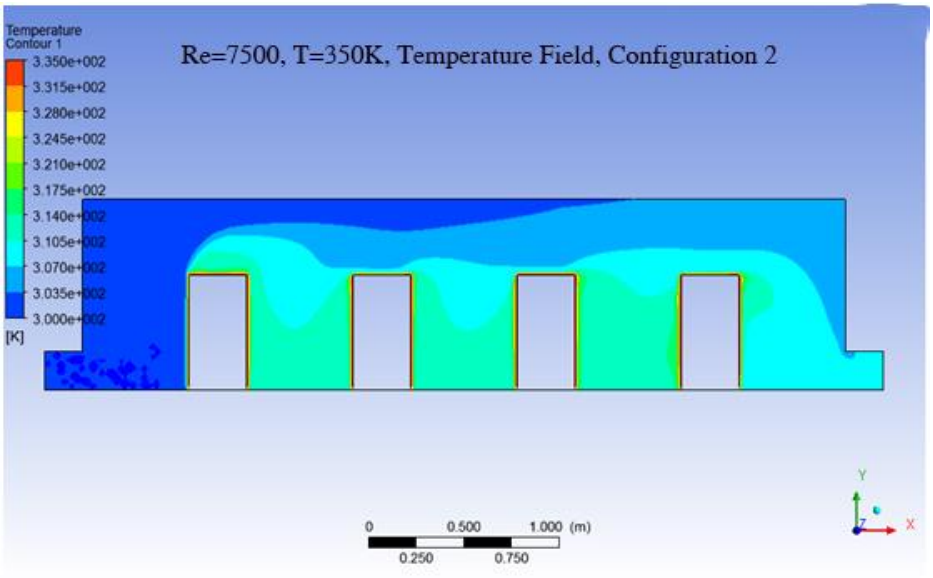

Figure 5.20. Temperature field of data center at Re = 7500 and server temperature (T) = 350K, configuration 2.

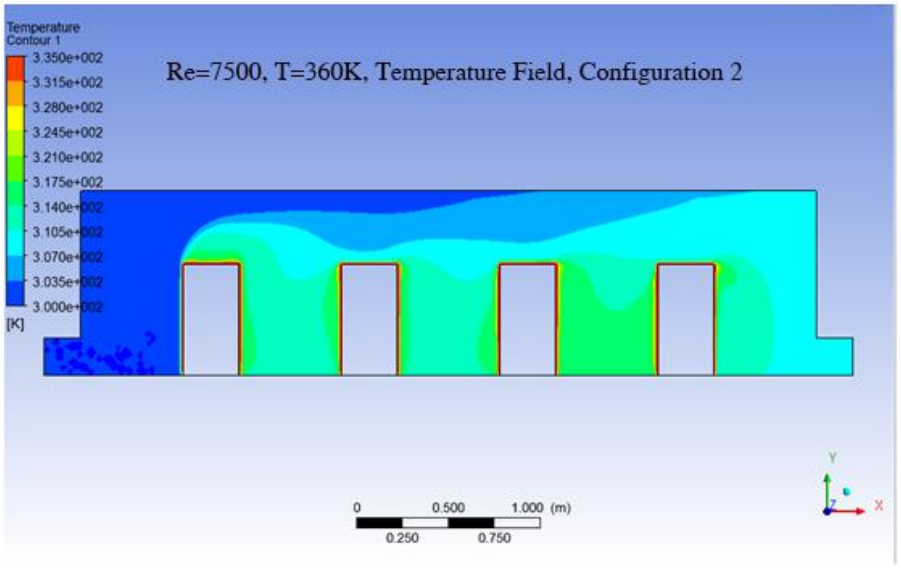

Figure 5.21. Temperature field of data center at Re = 7500 and server temperature (T) = 360K, configuration 2.

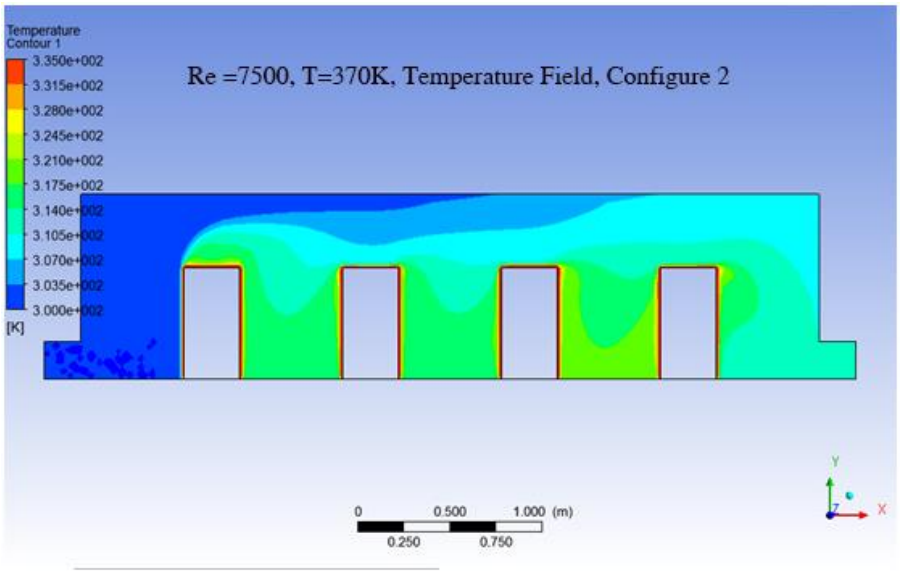

Figure 5.22. Temperature field of data center at Re = 7500 and server temperature (T) = 370K, configuration 2.

Figure 5.23 and Figure 5.24 give the velocity fields under the conditions of Re=7500 and the server temperature is taken as 370K in both configuration 1 and configuration 2. Comparing these two figures, we can find that the scale of vortex behind server 4 shrinks dramatically by converting from configuration 1 to configuration 2. A large vortex can

lead to flow stagnates, which can spoil the effects of heat convection because low temperature flow is blocked out. In Figure 5.24, since the vortex was broken down, the cooling effect on the server 4 was improved significantly. Not only in this case, but also in the practical designing process, it is necessary to keep breaking vortex in mind to reach better flow management in a data center.

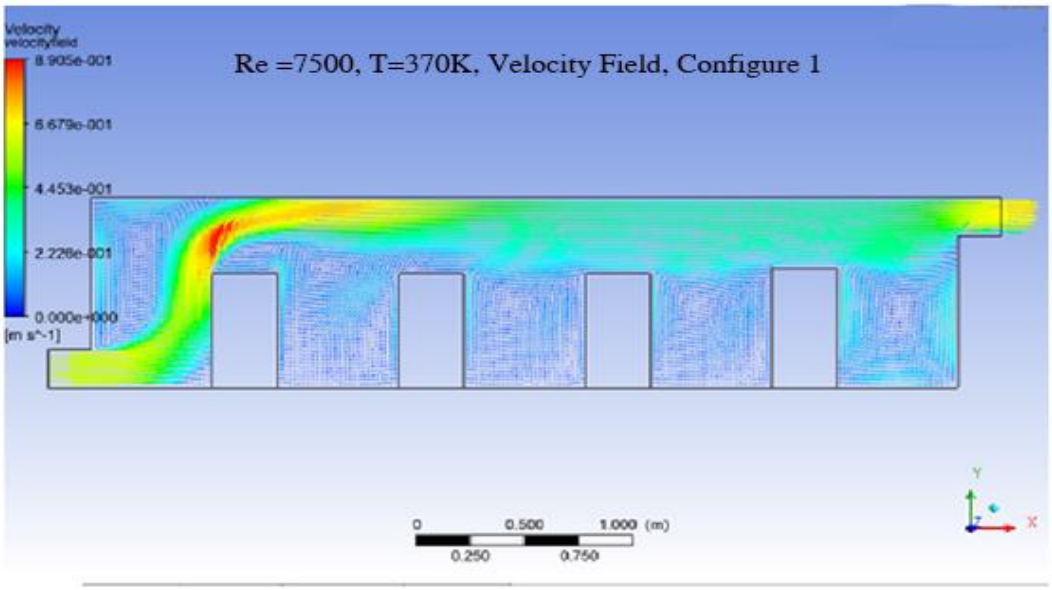

Figure 5.23. Velocity field of data center at Re = 7500 and server temperature (T) = 370K, configuration 1.

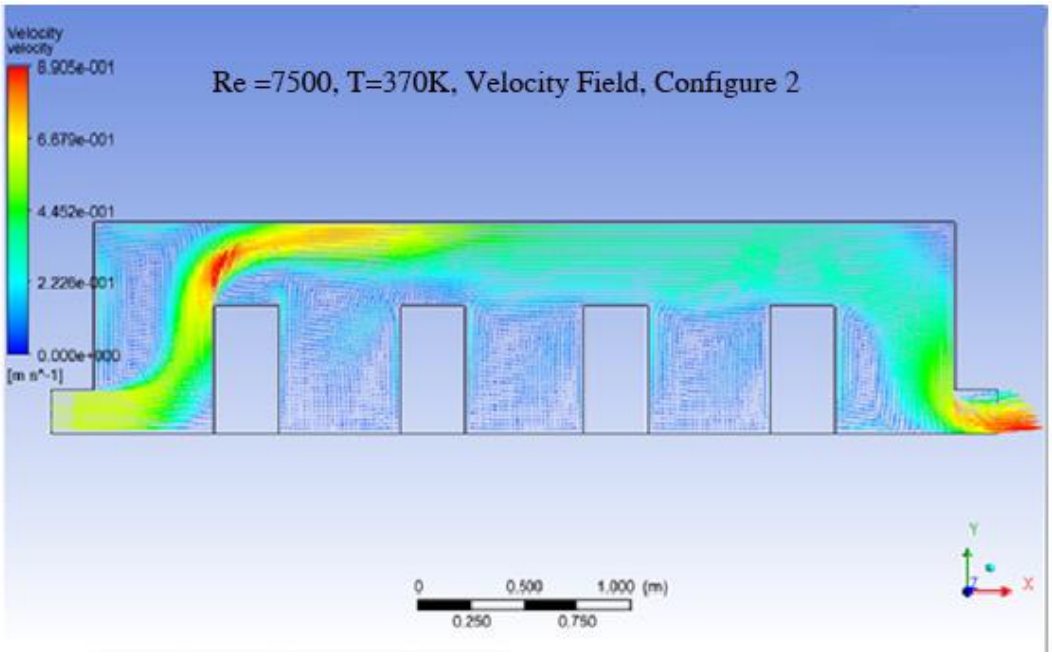

Figure 5.24. Velocity field of data center at Re = 7500 and server temperature (T) = 370K, configuration 2.

5.5 Transient cases

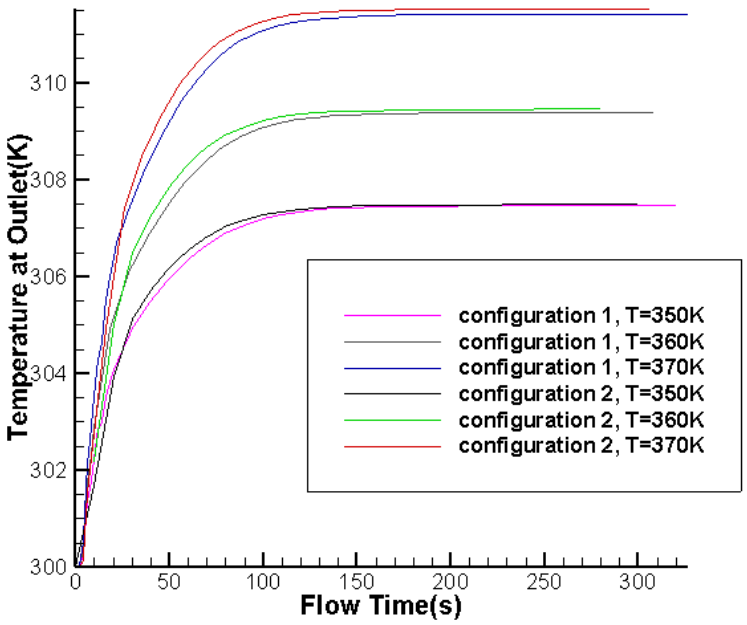

Figure 5.25 Transient cases, outlet average temperature as a function of time

Figure 5.25 gives us some insights into the average outlet temperature variation. The average temperature was gotten by Area-Weighted Average. At time = 0, the temperature at outlet is 300K, which is the ambient environment temperature. As time goes on, the average outlet temperature keeps increasing until reaching the static state outlet temperature. Comparing the average outlet temperature in configuration 1 and configuration 2 when server temperatures are the same, we can find that the average outlet temperature in configuration 2 is slightly higher than that in configuration 1. This phenomenon is the result of flow absorbing more heat energy from servers, especially from server 4, in configuration 2 than in configuration 1.

5.6 Configuration 3

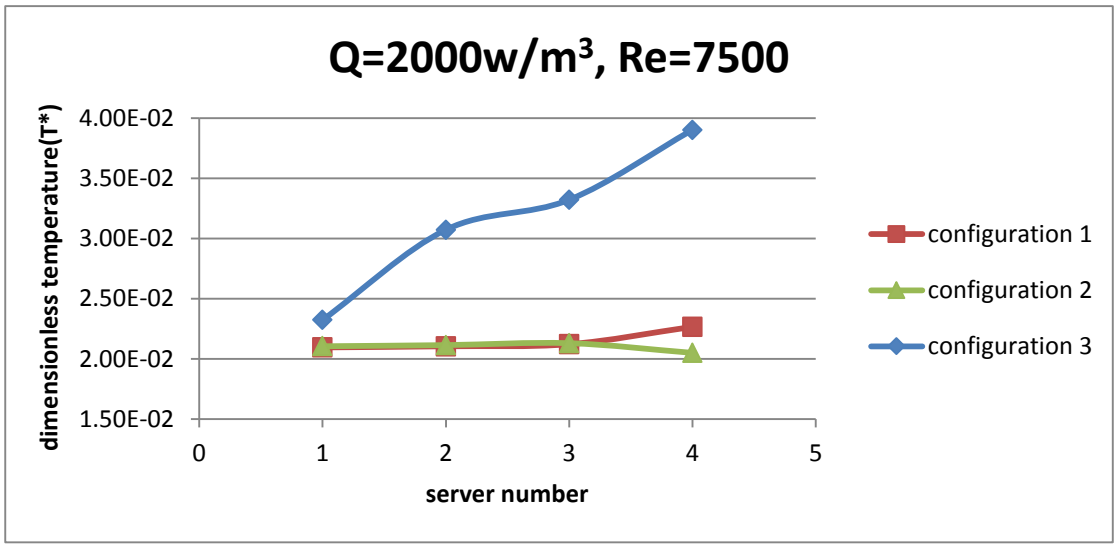

Figure 5.26. Server dimensionless temperature in different configurations at Re = 7500 and Q = 2000 w/m^3.

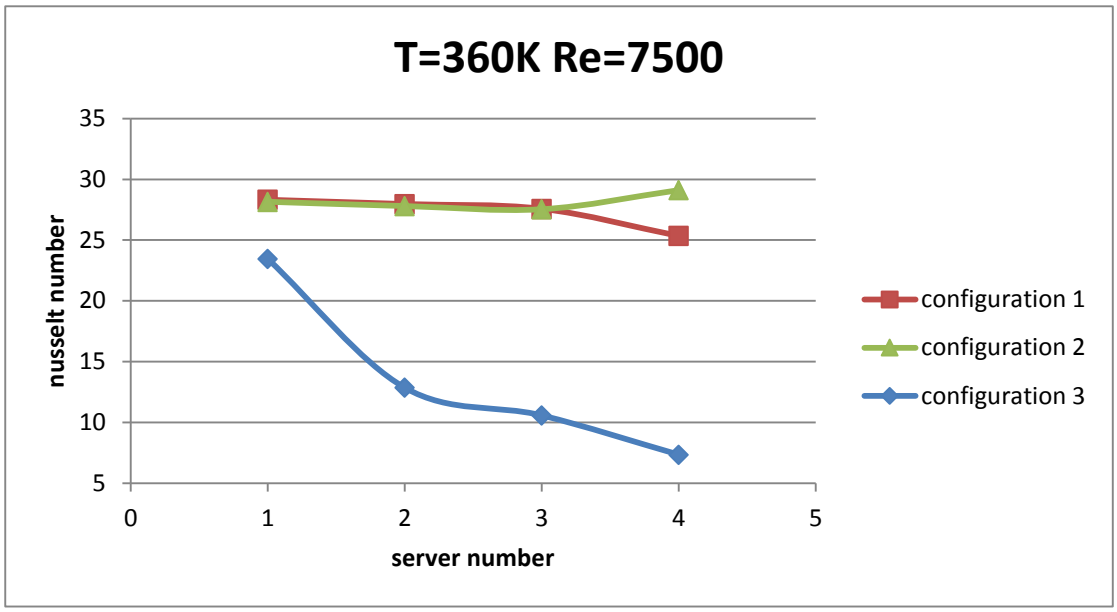

Figure 5.27. Servers' Nusselt number in different configurations at Re = 7500 and server temperature (T) = 360K.

Last but not least, the configuration 3 is discussed in this section. Configuration 3 is the case that inlet and outlet are at the same side of the data center, which costs least during building among all the three configurations. Figure 5.26 and Figure 5.27 give us some insights into configuration 3's performance. Figure 5.26 shows data center under the condition that Re=7500 and strength of volume heat sources Q=2000 w/m^3. The dimensionless temperature of servers in configuration 3 is much higher than that in configuration 1 and configuration 2. Figure 5.27 gives the Nu of servers in the data center when Re=7500 and server temperature=360K. The servers' Nu in configuration 3 is much lower than that of other configurations. As a result of understanding of the Figure 5.26 and Figure 5.27, it is not only inefficient but also dangerous to put the inlet and outlet at

the same side of data center, which should be avoid when designing a data center in practice.

6 Conclusions

After the analysis in section 5, here our conclusions are given.

Firstly, according to our simulation results, as the Re increasing at inlet, the cooling effect on servers improves reflected by servers' dimensionless temperature decreasing and Nu increasing. The servers located exterior, server 1 and server 4, are more sensitive to the flow velocity changing than servers located interior, server 2 and server 3.

Secondly, in this thesis, two configurations of data center are mainly compared. In configuration 1 the outlet is set at upper right hand side, and in configuration 2 the flow goes out the data center from down right corner. In configuration 1, the cooling effect on the server 4 is the worst among all the four servers in the data center. That phenomenon can be explained by the cooling flow keeps absorbing heat energy when successively flowing the servers, so when cooling flow passing the surfaces of server 4, its temperature is higher than the temperature when it passing other servers. While in configuration 2, the cooling effect on server 4 becomes the best comparing with other servers. By studying the temperature and velocity contours, we find that in configuration 2 the large vortex behind the server 4 is destroyed. As a result of that, the cooling flow can interact with the

surfaces of server 4 in a much more intense way. And since the flow absorbing more heat energy from server 4 in configuration 2 than that in configuration 1, the average outlet temperature in configuration 2 is slightly higher than that in configuration 1.

Last but not least, we also studied the performance of configuration 3, in which case the inlet and outlet are at the same side. We find the cooling effect, in terms of the dimensionless temperature and the Nu, are much worse that in configuration 1 and configuration 2. Thus, it is not only inefficient but also very dangerous to put the inlet and outlet at the same side when designing a data center.

References

[1] C.D. Patel, 2002, "Thermal Considerations in Cooling Large Scale High Compute Density Data Centers," The Eighth Intersociety Conference on Thermal and Thermomechanical Phenomena in Electronic System, 767-776.

[2] U.S Department of Energy, Retrieved 2014-6-20, "Data Center Energy Consumption Trends," http://energy.gov/eere/femp/data-center-energy-consumption-trends.

[3] U.S Environmental Protection Agency, 2007, "Report to Congress on Server and Data Center Energy Efficiency," Energy Star Program.

[4] M.K. Patterson, 2008, "The Effect of Data Center Temperature on Energy Efficiency," The Eleventh Intersociety Conference on Thermal and Thermomechanical Phenomena in Electronic Systems, 1167-1174.

[5] W. Tschudi, 2003, "Data Centers and Energy Use: Let's Look at the Data," ACEEE 2003 Paper#162

[6] C.D. Patel, 2001, "Computational Fluid Dynamics Modeling of High Compute Density Data Centers to Assure System Inlet Air Specifications," The Pacific Rim/ASME International Electronic Packaging Technical Conference and exhibition, IPACK2001-15622.

[7] K.C. Karki, 2003, "Use of Computational Fluid Dynamics for Calculating Flow Rates Through Perforated Tiles in Raised-Floor Data Centers," International Journal of Heating, Ventilation, Air-Conditioning, and Refrigeration Research, 9(2):153-166.

[8] J. Choi, 2008, "A CDF-Based Tool for Studying Temperature in Rack-Mounted Servers," IEEE Transactions on Computers, Vol. 57, No. 8.

[9] J. Choi, 2007, "Modeling and Managing Thermal Profiles of Rack-mounted Servers with ThermoStat," IEEE thirteenth International Symposium on High Performance Computer Architecture, 205-215.

[10] Y. Chen, 2005, "Managing Server Energy and Operational Costs in Hosting Centers," 2005 ACM SIGMETRICS International Conference on Measurement and Modeling of Computer Systems, 303-314.

[11] M. Lyengar, 2007, "Comparison between Numerical and Experimental Temperature Distributions in a Small Data Center Test Cell," ASME 2007 InterPACK Conference, Volume 1, 819-826.

[12] X. Zhang, 2008, "Effect of Rack Modeling Detail of the Numerical Results of a Data Center Test Cell," The Eleventh Intersociety Conference on Thermal and Thermomechanical Phenomena in Electronic Systems, 1183-1190.

[13] W.A. Abdelmaksoud, 2010, "Improved CFD Modeling of a Small Data Center Test Cell," The Twelfth Intersociety Conference on Thermal and Thermomechanical Phenomena in Electronic Systems,1-9.

[14] W.A. Abdelmaksoud, 2012, "Perforated Tile Models for Improving Data Center CFD Simulation," The Thirteenth Intersociety Conference on Thermal and Thermomechanical Phenomena in Electronic Systems, 60-67.

[15] J. Zhang, 2012, "Cooling of Electronic System: from Electronic Chips to Data Centers," PHD Thesis, Rutgers University.

[16] W. Lintner, 2010, "Best Practices Guide for Energy-Efficient Data Center Design," National Renewable Energy Laboratory (NREL), U.S. Department of Energy
[17] Buoyant Boussinesq Piso Foam, 2014-7-24, http://openfoamwiki.net/index.php/BuoyantBoussinesqPisoFoam

[18] B.E. Launder, 1974, "Application of the Energy Dissipation Model of Turbulence to the Calculation of Flow Near a Spinning Disc", Letters in Heat and Mass Transfer, vol. 1, no. 2, pp. 131-138.

[19] CFD Online, Retrived 2014-7-14, http://www.cfd-online.com/Wiki/Standard_k-epsilon_model.

[20] G. De Vahl Davis, 1983, "Natural Convection in a Square Cavity a Comparison Exercise," International Journal for Numerical Methods in Fluids, 3: 227-248.